CHINESE OPTICS LETTERS

Vol. 21, No. 4 | April 2023

Generation and application of high-contrast laser pulses using plasma mirror in the SULF-1PW beamline

Cheng Jiang (江 成)[1,†], Zongxin Zhang (张宗昕)[1,†], Hao Dong (董 浩)[1,2], Zhiyong Shi (史志勇)[1], Jianzhi He (何坚志)[1,2,3], Shufa Hao (郝书法)[1,2,3], Fengyu Sun (孙丰钰)[1,2,3], Jiayan Gui (归佳彦)[1], Jiayi Qian (钱佳毅)[1], Jiacheng Zhu (朱佳诚)[1], Wenpeng Wang (王文鹏)[1*], Yi Xu (许 毅)[1**], Xiaoyan Liang (梁晓燕)[1], Yuxin Leng (冷雨欣)[1***], and Ruxin Li (李儒新)[1,3]

[1] State Key Laboratory of High Field Laser Physics and CAS Center for Excellence in Ultra-intense Laser Science, Shanghai Institute of Optics and Fine Mechanics, Chinese Academy of Sciences, Shanghai 201800, China

[2] University of Chinese Academy of Sciences, Beijing 100049, China

[3] School of Physical Science and Technology, ShanghaiTech University, Shanghai 201210, China

*Corresponding author: wangwenpeng@siom.ac.cn

**Corresponding author: xuyi@siom.ac.cn

***Corresponding author: lengyuxin@mail.siom.ac.cn

Received September 14, 2022 | Accepted December 6, 2022 | Posted Online March 31, 2023

The plasma mirror system was installed on the 1 PW laser beamline of Shanghai Superintense Ultrafast Laser Facility (SULF) for enhancing the temporal contrast of the laser pulse. About 2 orders of magnitude improvement on pulse contrast was measured on picosecond and nanosecond time scales. The experiments show that high-contrast laser pulses can significantly improve the cutoff energy and quantity of proton beams. Then different target distributions are assumed in particles in cell simulations, which can qualitatively assume the expansion of nanometer-scale foil. The high-contrast laser enables the SULF-1PW beamline to generally be of benefit for many potential applications.

Keywords: ultraintense laser; plasma mirror; high-contrast laser; proton acceleration.

DOI: 10.3788/COL202321.043802

1. Introduction

With the development of chirped-pulse amplification (CPA) technology, numerous petawatt (PW)-class laser facilities have been constructed around the world[1], such as the BELLA laser[2], the J-KAREN-P laser[3], the ELI beamlines[4], and the Shanghai Superintense Ultrafast Laser Facility (SULF) beamlines[5,6]. The PW-class laser can produce focused laser intensities up to 10^{22}–10^{23} W/cm^2 for high-field physics applications[7–9]. At such high intensity levels, the temporal contrast of laser pulses has become one of the most important issues for laser–matter interaction experiments[10,11]. The temporal contrast is generally defined as the ratio of the intensity of the pedestal or subpeaks to the intensity of the main pulse[12]. The pedestal and subpeaks mainly include: (i) amplified spontaneous emission (ASE) on the nanosecond (ns) time scale; (ii) the pedestal on the picosecond (ps) time scale, arising from spectral clipping or modulation; and (iii) the pre-pulses on ps/ns time scales, originating from surface reflection or scattering[9,11]. The pedestal or subpeaks with intensities of 10^{10}–10^{11} W/cm^2 prior to the main pulse would ionize solid targets in laser–matter interactions[10,13].

Many techniques have been proposed and developed to improve the temporal contrast of high-power lasers, such as cross-polarized wave generation (XPW)[14], optical parametric amplification (OPA)[15], and plasma mirrors (PMs)[16–20]. Several approaches have been demonstrated in the SULF-1PW beamline before, such as the XPW and OPA filter[6]. Recently, a PM system was developed in the SULF-1PW beamline and tested for a proton acceleration experiment. For the PM, the substrate is usually a polished glass plate that is coated with a broadband antireflection coating[19]. When laser is focused on the surface of the PM, the low intensity pedestal or prepulses pass through the PM substrate with low reflectivity. Then the leading edge of the main pulse would ionize the surface of the PM substrate and generate the high-density plasma[21,22]. Therefore, the subsequent main pulse would be reflected by the high-density plasma surface[23]. The PM provides an ultrafast, self-induced optical switch for temporal contrast enhancement with the unlimited energy and power of the input laser.

In this paper, the characterization of the laser contrast using the PM system in the SULF-1PW beamline is reported. This PM system improves the temporal contrasts on ps and ns time scales by about 2 orders of magnitude. To evaluate the performance of

this system, we preliminarily performed proton acceleration contrast experiments. It shows that the proton beams accelerated by the high-contrast (HC, with PM system) laser have significantly improved cutoff energy and quantity compared to the low-contrast (LC, without PM system) case. In addition, simulation studies show that the target with a larger initial expansion scale (due to prepulse) had a lower cutoff energy of the proton beam. These results demonstrate that our PM system effectively improves the laser performance and can be well applied for laser-driven proton accelerations.

2. Experimental Setup

The experiments were carried out on the SULF-1PW beamline platform. The schematic of the PM system and the proton acceleration experiment is shown in Fig. 1. In experiments, the laser pulse duration was 27 fs at full width at half-maximum (FWHM), with an 800 nm center wavelength. The p-polarized laser beam was focused by using an *f*/4 off-axis parabola (OAP1) high-reflection mirror that had a 980 mm focal length with an off-axis angle of 20 deg. The PM substrate was clamped on a three-dimensional motorized translation stage placed in front of the focus position. It should be noted that the PM substrate used in our case was essentially a piece of fused silica glass whose surface was polished and coated with a broadband antireflection coating. The laser transmittance was greater than 99.5% when the PM was not excited. In order to avoid the effect of laser pulse reflected from the rear surface of the PM, the rear surface was also coated with the antireflection coating, and the wedge angle (3 deg) had been designed between the rear and front surfaces of the PM. In addition, the upper and lower parts of the PM were coated with reflective silver to facilitate alignment. After the PM, the divergent beam was recollimated into the parallel beam by OAP2, which had the same parameters as OAP1 and was placed symmetrically with OAP1. Subsequently, the temporal contrast-enhanced laser was reflected by mirror (R3) into the target chamber.

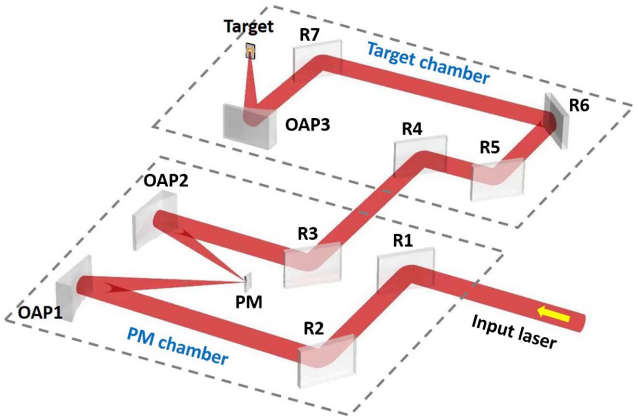

Fig. 1. Schematic of the experimental setup. R1–R7 are high-reflection dielectric mirrors; OAP1–OAP3 are off-axis parabola high-reflection mirrors.

The proton acceleration experiments were carried out in the target chamber. As shown in Fig. 1, the laser beam was finally focused by OAP3, which had a 998 mm focal length with an off-axis angle of 26 deg. The 50 nm thickness hydrocarbon target used in the experiment was placed at the laser focus, and the laser incident angle was 30 deg. The radiochromatic film (RCF) stack was placed behind the target at a distance of 80 mm from the target to measure the spatial intensity distribution of the proton beams. It was wrapped with a layer of 14 μm aluminum film to block the X-ray signal. A Thomson spectrometer was placed 420 mm away from the target in the normal direction. It should be noted that the R1 would be removed and R3 would reflect laser directly to target chamber by moving and rotating for the case without the PM.

3. Results

Before measuring the temporal contrast of the laser, it is necessary to find the optimal reflectivity efficiency of the PM used in our case, i.e., to measure the numerical relationship between the intensity of the focal spot on the surface of the PM and the reflectivity. The intensity of laser beam on the PM was varied from 1×10^{15} to 9×10^{15} W/cm^2 by adjusting the spot size on the surface by changing the distance between the PM and OAP1 while the input laser energy was fixed at ~13.5 J. The energy ratio of the reflected and incident beams of the PM system was measured for different intensity on the PM, as shown in Fig. 2. This indicates that the reflectivity reaches about 75% when the intensity is between 2.5×10^{15} W/cm^2 and 8.9×10^{15} W/cm^2 in our case. In addition, when the intensity was greater than 2×10^{16} W/cm^2, the far-field distribution of the reflected laser pulse was distorted, indicating that beam cannot be properly focused. The worse ability to focus may be owing to the distortion of phase front by the damaged PM surface, which can be caused by the several-picosecond rising edge of the main pulse[24] or by the prepulses, which were more than 10 ps prior to the main pulse[25]. Therefore, considering the wider variation range of input laser energy for flexible application requirements, the middle intensity of 5×10^{15} W/cm^2 was chosen, meaning

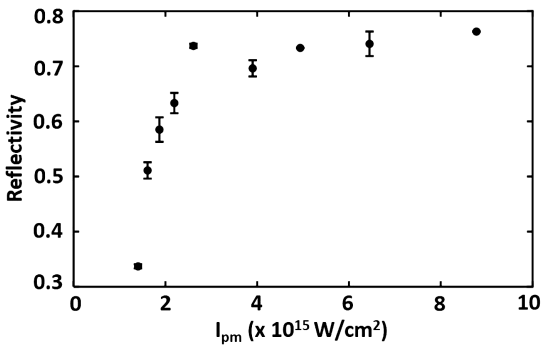

Fig. 2. Energy ratio of the reflected and incident laser beams of the PM system.

about 8 to 27 J of the input laser energy was allowed for our PM system.

The temporal contrasts on the ps time scale were measured by employing a high-dynamic-range third-order cross correlator (Sequoia, Amplitude Technologies), while the temporal contrasts on the ns time scale were measured by employing a fast photodiode (ET2030, Electro-Optics Technology) with neutral density filters. The measurement limits for the photodiode and Sequoia are 10^{-8} and 10^{-12}, respectively. The measurement results of temporal contrasts with PM and without PM are shown in Fig. 3. It should be noted that the temporal contrasts with PM were measured after R6, while the temporal contrasts without PM were measured with R1 removed and laser reflected directly to the target chamber, as mentioned at the end of the previous section. As shown in Fig. 3(a), three prepulses at −7.5, −11.3, and −15.7 ns were detected without using PM. Their temporal contrast ratios were $\sim 3.22 \times 10^{-8}$, $\sim 2.27 \times 10^{-8}$, and $\sim 4.07 \times 10^{-8}$, respectively. The prepulses were mainly generated from surface reflection or scattering in the amplifiers and compressor. By using PM, the prepulses were suppressed to an undetectable level, and the ASE pedestal was also suppressed effectively, as shown in Fig. 3(a). It could be estimated that the temporal contrast on the ns time scale was improved by about 2 orders of magnitude by the PM[22]. For the measurement of the temporal contrast on the ps time scale, the third-order cross correlator works by scanning data acquisition, i.e., one data point can be collected for one laser pulse. It can work well at fully automatic mode for the measurement of repetitive laser pulses. When the PM was employed, the surface of the PM irradiated by the laser would be ionized, and then the PM should be moved to a fresh surface for a subsequent laser pulse. Consequently, the third-order cross correlator had to work at the manual mode, which would limit the number of data points. Finally, the 30 discrete data points were collected, as shown in Fig. 3(b). Comparing the temporal contrasts on the ps time scale with and without the PM, it is not difficult to find that the PM system could suppress the ps scale pedestal by about 2 orders of magnitude, i.e., the temporal contrast at −2.8 ps was improved from $\sim 1.55 \times 10^{-6}$ to $\sim 2.03 \times 10^{-9}$. Therefore, the PM system can obviously improve the temporal contrast on both the ns and ps time scales, which has great significance for many physical experiments.

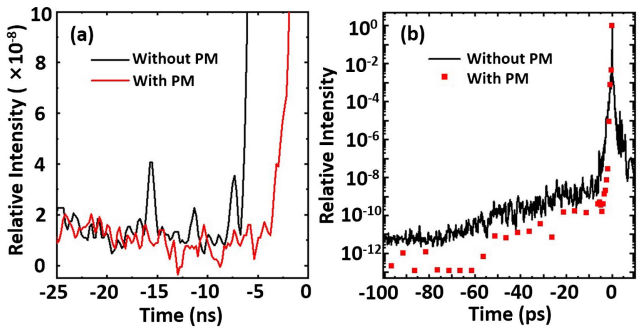

Fig. 3. Measured temporal contrasts without and with PM on the (a) ns time scale and (b) ps time scale.

The comparative studies were made with and without the PM system. The laser energy was fixed to ∼9 J on the target with a focal spot radius of ∼3 μm (FWHM), corresponding to the intensity of $\sim 5 \times 10^{20}$ W/cm^2. Figures 4(g) and 4(h) show the ion imaging trajectory collected by the energy spectrometer. The proton energy spectrum can be resolved, as shown in Fig. 4(i). This indicates that the cutoff energy of the proton beam obtained by the HC laser-driven acceleration is higher than in the LC case: the former reaches ∼9.2 MeV, while the latter is ∼6.1 MeV. In addition, the flux of the proton beam in the HC case, whose trajectories appeared saturated, as shown in Fig. 4(g), was significantly higher than that in the LC case, as shown in Fig. 4(h). This phenomenon was more apparent with RCF stacks, as shown in Figs. 4(a)–4(f). It also indicates that under the HC laser condition, the divergence of the proton beam was better than the LC laser results. The reason for the formation

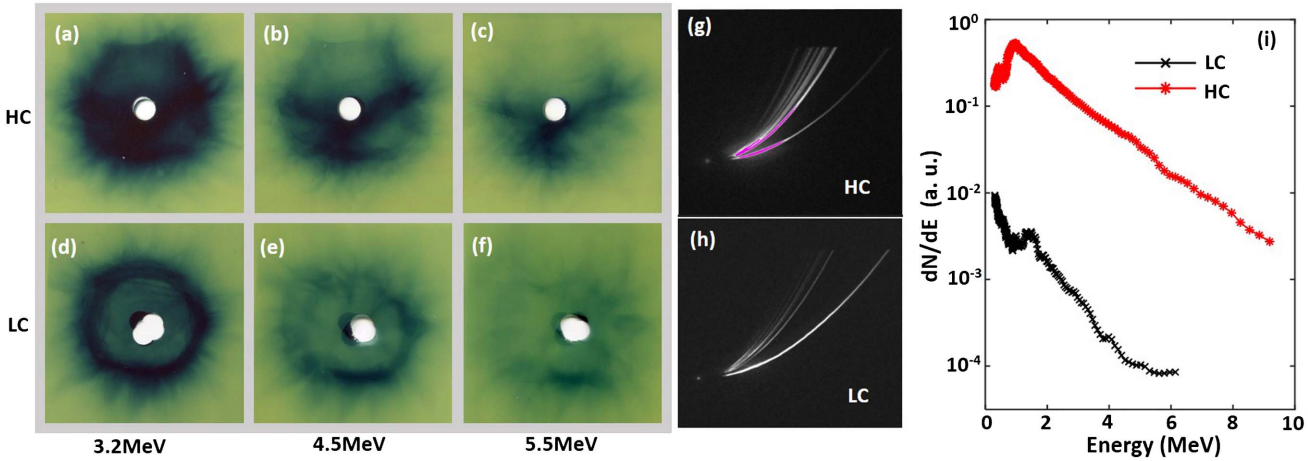

Fig. 4. (a)–(f) Proton beam spatial-intensity distribution for HC (a)–(c) and for LC (d)–(f) collected by the RCF stacks. The small hole in the middle of the RCF lets part of the particles pass through to be measured by ion spectroscopy. (g), (h) Ion imaging trajectories collected by the energy spectrometer for (g) HC and (h) LC laser conditions, respectively; (i) proton energy spectra solved from (g) and (h).

of an annular proton beam [see Figs. 4(d)–4(f)] may be the deformation and transverse nonuniform distribution of target caused by the prepulse[26]. It should be noted that the results of experiments are repeatable in our case. Such results showed that the laser contrast played an important role in the process of proton acceleration in our experiments.

4. Simulation and Discussion

The prepulses can affect the interaction when the main pulse irradiates on targets, because prepulses arrive at the target prior to the main pulse and expand the target. A combination of hydrodynamic codes and particle-in-cell (PIC) simulation to handle the whole interaction driven by prepulses and main pulses has been researched in previous studies[27]. However, for ultrathin solid targets with a thickness of tens of nanometers close to the molecular scale, it is not suitable for hydrodynamic simulations (at the ns scale) anymore[28,29]. Then, a simple model was used to estimate the effect of prepulses in our cases. The interaction of the femtosecond laser with different expanded targets was simulated by using the two-dimensional PIC code (EPOCH[30]).

The laser parameters in the PIC simulations were the same as those used in the experiments. The size of the simulation box is 24 μm (x) × 24 μm (y) with 3840 × 1920 cells, and each cell was filled with 20 particles. The incident angle of laser was 30 deg. The targets are modeled by cold plasmas composed of C^{4+}, protons, and electrons, where the ratio of C^{4+} to proton was 1:2. In the ideal case, the thickness of the unexpanded target was 50 nm, and the proton number density was $94.6n_c$ with uniform distribution, where $n_c = 1.75 \times 10^{21}$ cm^{-3} was the critical density for 800 nm of laser wavelength. However, due to effect of the prepulse, we assume that the expanded target density distribution was a Gaussian function before the main pulse arrives. It can be expressed as $n_p(l) = n_0 \exp[-4 \ln(2) l^2/L^2]$, where l is the distance from the center of the target, L is the thickness at FWHM, and n_0 is the maximum density. The total number of protons in the target was kept as constant for different simulations, i.e., $\int n_p(l)\mathrm{d}l = 50\ \mathrm{nm} \times 94.6n_c$. Therefore, the $L = 0.1$ μm ($n_0 = 44.6n_c$), 0.5 μm ($n_0 = 8.92n_c$), 1.5 μm ($n_0 = 2.97n_c$), 5 μm ($n_0 = 0.892n_c$) cases, and an ideal unexpanded case were simulated, respectively.

The energy spectrum from the PIC simulations is shown in Fig. 5. When the initial expanded size of the target was small, the proton cutoff energy was around 14 MeV for the cases of $L = 0.1$ μm, 0.5 μm expansion targets, and the ideal unexpanded target. However, while the expanded size of the target increased, the cutoff energy of protons became smaller. For example, the $L = 1.5$ μm and 5 μm expansions corresponded to cutoff energies of 10 and 5.6 MeV, respectively. Such results were close to the proton energy spectra from the HC and LC cases [as shown in Fig. 4(i)] in the experiments. Because the target parameters in PIC simulation were estimated by the simplified model, the simulation results could not be strictly used as the quantitative basis for the experimental results. However, it could be

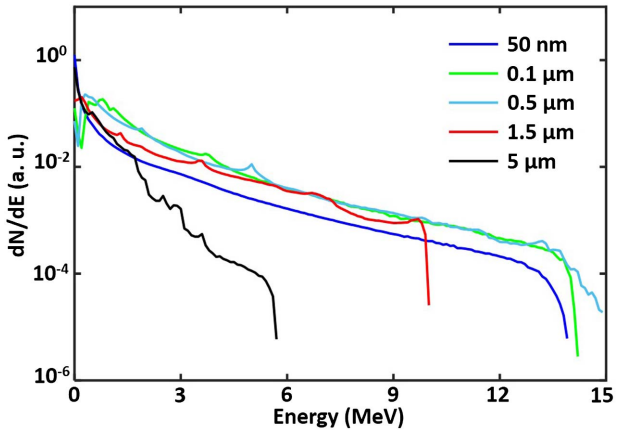

Fig. 5. Energy spectrum of the proton with the different pre-ionized expanded targets from PIC simulations at ~107 fs after the laser arrived at the front surface of the target. The thickness of the ideal unexpanded target was 50 nm (blue line) with uniform density distribution. The density of the Gaussian function distribution was considered for expanded target cases with thickness (FWHM) of 0.1 μm (green line), 0.5 μm (light blue line), 1.5 μm (red line) and 5 μm (black line).

explained that the proton energy was reduced due to the larger expansion of the target in experiments. We note that under the conditions of our experiments and simulations, the proton was accelerated by the target normal sheath acceleration (TNSA) mechanism[13]. The appropriate plasma gradient was beneficial to laser absorption of electrons, which would enhance the effect of TNSA[31]. Therefore, the proton cutoff energy of the 0.1 and 0.5 μm targets with plasma gradient was higher than that of the 50 nm target without plasma gradient in PIC simulations. However, the larger expansion of the target would induce the smaller density gradient at the rear surface, resulting in a weaker sheath electric field, thereby reducing the acceleration effect of the TNSA[32]. Therefore, the LC laser greatly increases the expansion of the target, detrimental to the TNSA, leading to the lower cutoff energy, which is consistent with the experimental results in Fig. 4.

5. Summary

In conclusion, this paper reports the characterization of the laser contrast using the PM system in the SULF-1PW beamline. This PM system enhances the temporal contrasts on ps and ns time scales by about 2 orders of magnitude. The experiments with proton acceleration also verified that the use of this system can significantly improve the cutoff energy and quantity of proton beams. The simulation can qualitatively predict the expansion of the target with HC and LC lasers. The LC prepulse would greatly increase the expansion of the target, which is bad for proton accelerations. To solve this issue, the PM system is designed to effectively improve the laser contrast in our case. With the progress of PM technology, experiments have shown that PM reflectivity can reach 95%[33], effectively improving the laser energy on target. It is also expected to effectively alleviate the

problem of high energy loss in the cascade use of multiple PMs, providing a robust and efficient tool for research on particle acceleration, solid high-order harmonics, and attosecond radiation.

Acknowledgement

We thank Dr. Xiaohui Yuan and Dr. Xulei Ge for useful comments and discussion. This work was supported by the National Natural Science Foundation of China (No. 12075306), the Natural Science Foundation of Shanghai (No. 22ZR1470900), the Key Research Programs in Frontier Science (No. ZDBS-LY-SLH006), and the China Postdoctoral Science Foundation (No. 2021M703328).

†These authors contributed equally to this work.

References

1. C. Danson, D. Hillier, N. Hopps, and D. Neely, "Petawatt class lasers worldwide," High Power Laser Sci. Eng. **3**, e3 (2015).
2. K. Nakamura, H.-S. Mao, A. J. Gonsalves, H. Vincenti, D. E. Mittelberger, J. Daniels, A. Magana, C. Toth, and W. P. Leemans, "Diagnostics, control and performance parameters for the BELLA high repetition rate petawatt class laser," IEEE J. Quantum Electron. **53**, 1200121 (2017).
3. H. Kiriyama, A. S. Pirozhkov, M. Nishiuchi, Y. Fukuda, K. Ogura, A. Sagisaka, Y. Miyasaka, M. Mori, H. Sakaki, N. P. Dover, K. Kondo, J. K. Koga, T. Z. Esirkepov, M. Kando, and K. Kondo, "High-contrast high-intensity repetitive petawatt laser," Opt. Lett. **43**, 2595 (2018).
4. F. Lureau, G. Matras, O. Chalus, C. Derycke, T. Morbieu, C. Radier, O. Casagrande, S. Laux, S. Ricaud, G. Rey, A. Pellegrina, C. Richard, L. Boudjemaa, C. Simon-Boisson, A. Baleanu, R. Banici, A. Gradinariu, C. Caldararu, B. De Boisdeffre, P. Ghenuche, A. Naziru, G. Kolliopoulos, L. Neagu, R. Dabu, I. Dancus, and D. Ursescu, "High-energy hybrid femtosecond laser system demonstrating 2 × 10 PW capability," High Power Laser Sci. Eng. **8**, e43 (2020).
5. W. Li, Z. Gan, L. Yu, C. Wang, Y. Liu, Z. Guo, L. Xu, M. Xu, Y. Hang, Y. Xu, J. Wang, P. Huang, H. Cao, B. Yao, X. Zhang, L. Chen, Y. Tang, S. Li, X. Liu, S. Li, M. He, D. Yin, X. Liang, Y. Leng, R. Li, and Z. Xu, "339 J high-energy Ti:sapphire chirped-pulse amplifier for 10 PW laser facility," Opt. Lett. **43**, 5681 (2018).
6. Z. Zhang, F. Wu, J. Hu, X. Yang, J. Gui, P. Ji, X. Liu, C. Wang, Y. Liu, X. Lu, Y. Xu, Y. Leng, R. Li, and Z. Xu, "The 1 PW/0.1 Hz laser beamline in SULF facility," High Power Laser Sci. Eng. **8**, e4 (2020).
7. T. J. Yu, S. K. Lee, J. H. Sung, J. W. Yoon, T. M. Jeong, and J. Lee, "Generation of high-contrast, 30 fs, 1.5 PW laser pulses from chirped-pulse amplification Ti:sapphire laser," Opt. Express **20**, 10807 (2012).
8. J. W. Yoon, Y. G. Kim, I. W. Choi, J. H. Sung, H. W. Lee, S. K. Lee, and C. H. Nam, "Realization of laser intensity over 1023 W/cm^2," Optica **8**, 630 (2021).
9. D.-Q. Wen, P. Zhang, J. Krek, Y. Fu, and J. P. Verboncoeur, "Higher harmonics in multipactor induced plasma ionization breakdown near a dielectric surface," Phys. Rev. Lett. **129**, 045001 (2022).
10. H. Kiriyama, Y. Miyasaka, A. Sagisaka, K. Ogura, M. Nishiuchi, A. S. Pirozhkov, Y. Fukuda, M. Kando, and K. Kondo, "Experimental investigation on the temporal contrast of pre-pulses by post-pulses in a petawatt laser facility," Opt. Lett. **45**, 1100 (2020).
11. L. Ranc, C. Le Blanc, N. Lebas, L. Martin, J. P. Zou, F. Mathieu, C. Radier, S. Ricaud, F. Druon, and D. Papadopoulos, "Improvement in the temporal contrast in the tens of ps range of the multi-PW Apollon laser front-end," Opt. Lett. **45**, 4599 (2020).
12. K. Osvay, M. Csatári, I. N. Ross, A. Persson, and C.-G. Wahlström, "On the temporal contrast of high intensity femtosecond laser pulses," Laser Part. Beams **23**, 327 (2005).
13. M. Kaluza, J. Schreiber, M. I. Santala, G. D. Tsakiris, K. Eidmann, J. Meyer-ter-Vehn, and K. J. Witte, "Influence of the laser prepulse on proton acceleration in thin-foil experiments," Phys. Rev. Lett. **93**, 045003 (2004).
14. A. Jullien, O. Albert, F. Burgy, G. Hamoniaux, J.-P. Rousseau, J.-P. Chambaret, F. Augé-Rochereau, G. Chériaux, J. Etchepare, N. Minkovski, and S. M. Saltiel, "10^{-10} temporal contrast for femtosecond ultraintense lasers by cross-polarized wave generation," Opt. Lett. **30**, 920 (2005).
15. C. Dorrer, I. A. Begishev, A. V. Okishev, and J. D. Zuegel, "High-contrast optical-parametric amplifier as a front end of high-power laser systems," Opt. Lett. **32**, 2143 (2007).
16. C. Thaury, F. Quéré, J. P. Geindre, A. Levy, T. Ceccotti, P. Monot, M. Bougeard, F. Réau, P. d'Oliveira, P. Audebert, R. Marjoribanks, and P. Martin, "Plasma mirrors for ultrahigh-intensity optics," Nat. Phys. **3**, 424 (2007).
17. A. Lévy, T. Ceccotti, P. D'Oliveira, F. Réau, M. Perdrix, F. Quéré, P. Monot, M. Bougeard, H. Lagadec, and P. Martin, "Double plasma mirro for ultrahigh temporal contrast ultraintense laser pulses," Opt. Lett. **32**, 310 (2007).
18. Y. Nomura, L. Veisz, K. Schmid, T. Wittmann, J. Wild, and F. Krausz, "Time-resolved reflectivity measurements on a plasma mirror with few-cycle laser pulses," New J. Phys. **9**, 9 (2007).
19. S. Inoue, K. Maeda, S. Tokita, K. Mori, K. Teramoto, M. Hashida, and S. Sakabe, "Single plasma mirror providing 104 contrast enhancement and 70% reflectivity for intense femtosecond lasers," Appl. Opt. **55**, 5647 (2016).
20. L. Obst, J. Metzkes-Ng, S. Bock, G. E. Cochran, T. E. Cowan, T. Oksenhendler, P. L. Poole, I. Prencipe, M. Rehwald, C. Rödel, H. P. Schlenvoigt, U. Schramm, D. W. Schumacher, T. Ziegler, and K. Zeil, "On-shot characterization of single plasma mirror temporal contrast improvement," Plasma Phys. Control. Fusion **60**, 054007 (2018).
21. B. Dromey, S. Kar, M. Zepf, and P. Foster, "The plasma mirror—a subpicosecond optical switch for ultrahigh power lasers," Rev. Sci. Instrum. **75**, 645 (2004).
22. I. W. Choi, C. Jeon, S. G. Lee, S. Y. Kim, T. Y. Kim, I. J. Kim, H. W. Lee, J. W. Yoon, J. H. Sung, S. K. Lee, and C. H. Nam, "Highly efficient double plasma mirror producing ultrahigh-contrast multi-petawatt laser pulses," Opt. Lett. **45**, 6342 (2020).
23. X. G. Ge, Y. Fang, S. Yang, W. Wei, F. Liu, P. Yuan, J. Ma, L. Zhao, X. Yuan, and J. Zhang, "Characterization and application of plasma mirror for ultraintense femtosecond lasers," Chin. Opt. Lett. **16**, 013201 (2018).
24. C. Rödel, M. Heyer, M. Behmke, M. Kübel, O. Jäckel, W. Ziegler, D. Ehrt, M. C. Kaluza, and G. G. Paulus, "High repetition rate plasma mirror for temporal contrast enhancement of terawatt femtosecond laser pulses by three orders of magnitude," Appl. Phys. B **103**, 295 (2011).
25. G. G. Scott, V. Bagnoud, C. Brabetz, R. J. Clarke, J. S. Green, R. I. Heathcote, H. W. Powell, B. Zielbauer, T. D. Arber, P. McKenna, and D. Neely, "Optimization of plasma mirror reflectivity and optical quality using double laser pulses," New J. Phys. **17**, 033027 (2015).
26. M. H. Xu, Y. T. Li, X. H. Yuan, Q. Z. Yu, S. J. Wang, W. Zhao, X. L. Wen, G. C. Wang, C. Y. Jiao, Y. L. He, S. G. Zhang, X. X. Wang, W. Z. Huang, Y. Q. Gu, and J. Zhang, "Effects of shock waves on spatial distribution of proton beams in ultrashort laser-foil interactions," Phys. Plasmas **13**, 104507 (2006).
27. W. P. Wang, C. Jiang, H. Dong, X. M. Lu, J. F. Li, R. J. Xu, Y. J. Sun, L. H. Yu, Z. Guo, X. Y. Liang, Y. X. Leng, R. X. Li, and Z. Z. Xu, "Hollow plasma acceleration driven by a relativistic reflected hollow laser," Phys. Rev. Lett. **125**, 034801 (2020).
28. R. Ramis, K. Eidmann, J. Meyer-ter-Vehn, and S. Hüller, "Multi-fs–a computer code for laser–plasma interaction in the femtosecond regime," Comput. Phys. Commun. **183**, 637 (2012).
29. Y. Kuramitsu, T. Minami, T. Hihara, K. Sakai, T. Nishimoto, S. Isayama, Y. T. Liao, K. T. Wu, W. Y. Woon, S. H. Chen, Y. L. Liu, S. M. He, C. Y. Su, M. Ota, S. Egashira, A. Morace, Y. Sakawa, Y. Abe, H. Habara, R. Kodama, L. N. K. Döhl, N. Woolsey, M. Koenig, H. S. Kumar, N. Ohnishi, M. Kanasaki, T. Asai, T. Yamauchi, K. Oda, Ko. Kondo, H. Kiriyama, and Y. Fukuda, "Robustness of large-area suspended graphene under interaction with intense laser," Sci. Rep. **12**, 2346 (2022).
30. T. D. Arber, K. Bennett, C. S. Brady, A. Lawrence-Douglas, M. G. Ramsay, N. J. Sircombe, P. Gillies, R. G. Evans, H. Schmitz, A. R. Bell, and C. P. Ridgers, "Contemporary particle-in-cell approach to laser-plasma modelling," Plasma Phys. Control. Fusion **57**, 113001 (2015).

31. A. A. Andreev, R. Sonobe, S. Kawata, S. Miyazaki, K. Sakai, K. Miyauchi, T. Kikuchi, K. Platonov, and K. Nemoto, "Effect of a laser prepulse on fast ion generation in the interaction of ultra-short intense laser pulses with a limited-mass foil target," Plasma Phys. Control. Fusion **48**, 1605 (2006).
32. W. P. Wang, H. Zhang, B. Wu, C. Y. Jiao, Y. C. Wu, B. Zhu, K. G. Dong, W. Hong, Y. Q. Gu, B. F. Shen, Y. Xu, Y. X. Leng, R. X. Li, and Z. Z. Xu, "Generation of low-divergence megaelectronvolt ion beams from thin foil irradiated with an ultrahigh-contrast laser," Appl. Phys. Lett. **101**, 214103 (2012).
33. G. G. Scott, G. F. H. Indorf, M. A. Ennen, P. Forestier-Colleoni, S. J. Hawkes, L. Scaife, M. Sedov, D. R. Symes, C. Thornton, F. Beg, T. Ma, P. McKenna, A. A. Andreev, U. Teubner, and D. Neely, "Kinematics of femtosecond laser-generated plasma expansion: determination of sub-micron density gradient and collisionality evolution of over-critical laser plasmas," Phys. Plasmas **28**, 093109 (2021).